Electronic Supplementary Information

Photoabsorption of silver cluster cations in an ion trap: nonlinear action spectra via multi-photon dissociation vs. directly-measured linear absorption spectra

Satoshi Kono, Shuhei Fujimoto, Tomonori Ito, Masashi Arakawa,† Takuya Horio and Akira Terasaki*

Department of Chemistry, Faculty of Science, Kyushu University, 744 Motooka, Nishi-ku, Fukuoka 819-0395, Japan. E-mail: terasaki@chem.kyushu-univ.jp.

† Present address: *Department of Earth and Planetary Sciences, Faculty of Science, Kyushu University, 744 Motooka, Nishi-ku, Fukuoka 819-0395, Japan.*

1. Ion trap

1.1. Configuration

A homemade linear ion trap[1] was employed in this study, which consists of an octopole ion guide arranged between two end electrodes (Figure S1a). The ion guide was driven by radio-frequency (rf) voltages from a homemade rf generator[2] for radial confinement of ions, while axial confinement was controlled by DC voltages applied to the end electrodes with the aid of a buffer He gas to decelerate the ions in the trap. As depicted in Figure S1b, the eight pole electrodes (ϕ = 3 mm) were arranged in a circular manner with an inscribed circle diameter of 11 mm. The ion guide was operated in a quadrupole mode by wiring neighboring poles pairwise to form four pairs of electrodes, which concentrated the ions to distribute near the center of the trap, ensuring optimal overlap between the ions and a laser beam; otherwise, an ordinary octopole forces the ions distributed in a ring profile with a low ion density on the axis of the trap.[3]

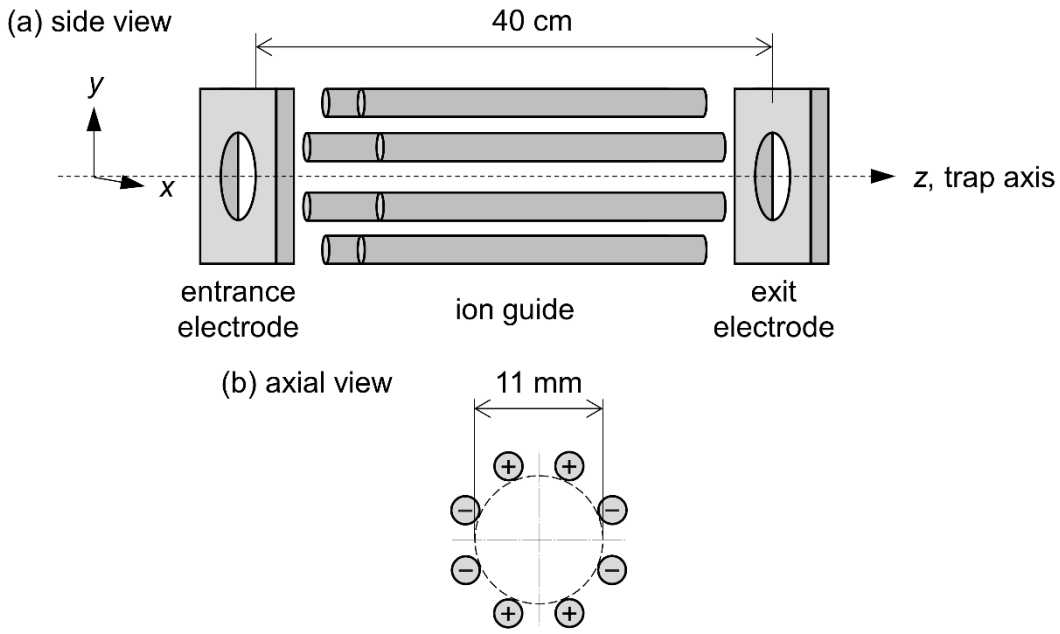

Figure S1. A schematic view of the present ion trap.

1.2. Evaluation of overlap between ions and laser beam

The spatial distribution of the ion density is a key to quantitative evaluation of photodissociation cross sections, which was measured prior to experiment of photodissociation spectroscopy. The procedure has been described elsewhere.[3] Briefly, dissociation yields were measured by scanning the laser position (x, y) at a constant laser power. The spot size, ~1 mm in diameter, of the laser beam was also kept constant during the measurement. The result was typically Gaussian-like as shown in Figure S2 measured for Ag_3^+ in the quadrupole-mode operation of the present ion trap. This one-dimensional result was converted to two-dimensional data by assuming a cylindrical symmetry. Numerical integration of the two-dimensional data within the spot size of the laser beam in the spectrum measurements (typically about 3 mm in diameter) gives the γ value, i.e., the fraction of the ions irradiated with the laser, in Equation 1.

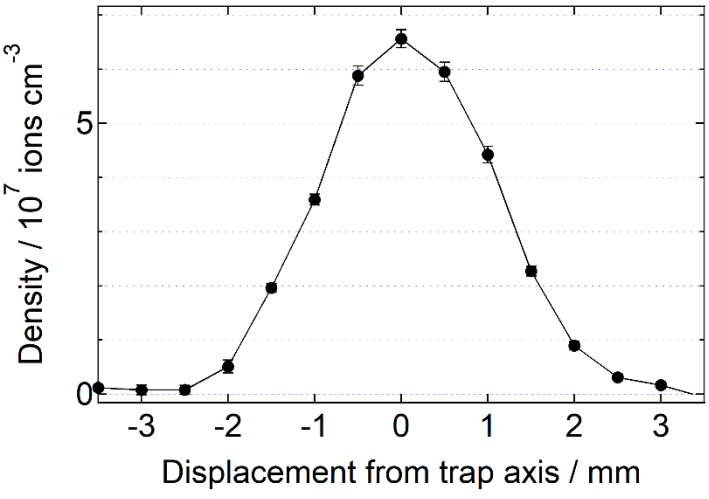

Figure S2. Spatial distribution of Ag_3^+ inside the trap.

2. Photon-energy dependence of dissociation process

The dissociation processes of silver clusters are dependent on photon energy as well as cluster sizes. The photodissociation spectrum of Ag_{18}^{+} is shown in Figure S3a for example. The ordinate shows dissociation yields per photon, D / N_{photon}, instead of photodissociation cross sections because one- and two-photon dissociation processes coexist in the spectrum. The coexistence of the two dissociation processes were confirmed by an additional experiment shown in Figure S3b, which displays the dissociation yield measured as a function of the number of incident photons at three photon energies indicated by the arrows in Figure S3a. Firstly, the value of the slope is M = 1.00 ± 0.04 at 4.25 eV, indicating one-photon dissociation at this photon energy. The slope becomes steeper as the photon energy is lowered, where the M value is between one and two; M = 1.40 ± 0.03 at 4.00 eV. This non-integer slope suggests that both one- and two-photon dissociation channels are present. The M value finally reaches 2.1 ± 0.1 at 3.00 eV, indicating two-photon dissociation as a major process. This photon-energy dependence of the dissociation processes was also observed for N = 15 and 17. On the other hand, N = 16 exhibited only one-photon dissociation in the corresponding spectral range.

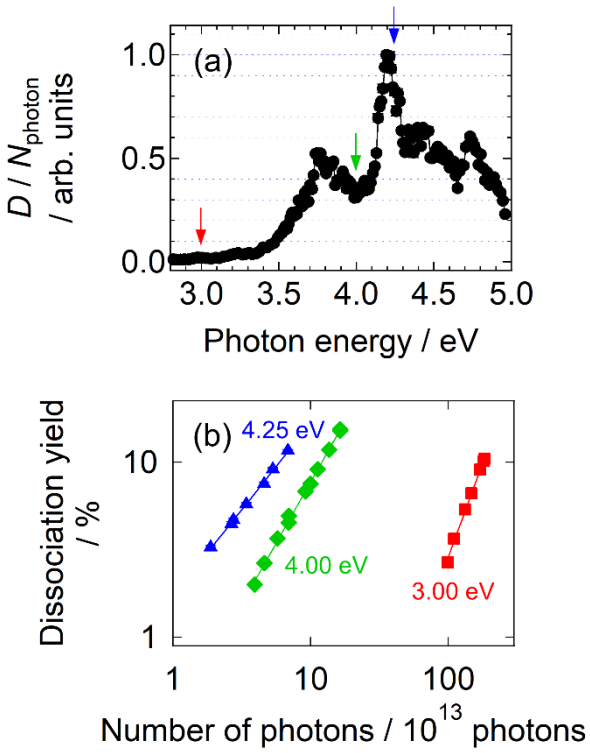

Figure S3. (a) The photodissociation spectrum of Ag_{18}^{+}. (b) The photodissociation yield of Ag_{18}^{+} as a function of the number of the incident photons in 10 pulses. The measurement was performed at three energies of incident photons indicated by colored arrows in Panel (a). The solid lines are the best linear fits to the logarithmic plots. The values of the slopes are $M = 2.1 \pm 0.1$, 1.40 ± 0.03 and 1.00 ± 0.04 for 3.00, 4.00 and 4.25 eV, respectively. The pressure and the temperature of the buffer gas were ~ 1 Pa and 300 K, respectively.

3. Simulation of photodissociation processes

3.1. Method

The statistical RRK theory[4–6] is employed to estimate the dissociation rate upon photoabsorption, which is expressed by the following equation:

$$k_{\mathrm{RRK}} = \begin{cases} \nu\left(1 - \dfrac{D_0}{E_{\mathrm{int}}}\right)^{s-1} & (D_0 \le E_{\mathrm{int}}) \\ 0 & (\text{otherwise}) \end{cases}, \qquad \text{(S1)}$$

where ν is the frequency pre-factor, E_{int} the internal energy of the cluster, D_0 the bond-dissociation energy and s the number of the vibrational modes that is $3N - 5$ (for linear clusters, i.e., the dimer) or $3N - 6$ (for the others). The bond dissociation energy, D_0, has been reported by collision-induced dissociation[7] and time-resolved photofragmentation[8] experiments, which also employed a statistical theory for analysis. The internal energy E_{int} originates from the initial thermal energy due to the temperature and from the photon energy absorbed. Eqn (S1) tells that the cluster would dissociate when E_{int} exceeds D_0 upon absorption of a photon with a sufficiently high energy and that the dissociation rate decreases exponentially as the cluster size N increases. Therefore, once E_{int} exceeds D_0, one-photon dissociation should be observed even for large clusters if the clusters were stored in the trap for sufficiently long time in accordance with the lowered dissociation rate. However, practically, the clusters release their internal energy via cooling upon collision with the buffer gas, which could suppress dissociation of large clusters if the cooling rate exceeds the dissociation rate. In such a case, clusters absorb multiple photons to increase their internal energies, which accelerates dissociation. This is the qualitative explanation for the multi-photon dissociation observed at large cluster sizes.

For quantitative understanding, numerical simulation was performed as follows. Suppose that all the clusters are photoexcited and that the photon energy absorbed is all converted to the internal energy of the clusters via rapid internal conversion followed by IVR. The density of the parent cluster, $n_{\mathrm{parent}}(t)$, at time, t, after laser irradiation follows the following differential equation:

$$\frac{\mathrm{d}n_{\mathrm{parent}}(t)}{\mathrm{d}t} = -k_{\mathrm{RRK}}(t)\, n_{\mathrm{parent}}(t). \tag{S2}$$

$k_{\mathrm{RRK}}(t)$ is the unimolecular RRK decay rate of eqn (S1) modified to include time dependence:

$$k_{\mathrm{RRK}}(t) = \begin{cases} v\left(1 - \dfrac{D_0}{E_{\mathrm{int}}(t)}\right)^{s-1} & (D_0 \le E_{\mathrm{int}}(t)) \\ 0 & (\text{otherwise}) \end{cases}, \tag{S3}$$

where $E_{\mathrm{int}}(t)$ is the time-dependent internal energy, which takes into account collisional cooling as follows:

$$E_{\mathrm{int}}(t) = \begin{cases} sk_{\mathrm{B}}T_{\mathrm{buffer}} + h\nu \equiv sk_{\mathrm{B}}T_{\mathrm{parent}}(0) & (t = 0) \\ sk_{\mathrm{B}}T_{\mathrm{parent}}(t) & (t > 0) \end{cases} \tag{S4}$$

by assuming one-photon absorption, where k_{B} is Boltzmann's constant and $T_{\mathrm{parent}}(t)$ the temperature of the cluster. According to Ref. 9, $T_{\mathrm{parent}}(t)$ is expressed by

$$T_{\mathrm{parent}}(t) = \left(T_{\mathrm{parent}}(0) - T_{\mathrm{buffer}}\right)\left(1 - \frac{K}{3Nk_{\mathrm{B}}}\right)^{\frac{t}{t_{\mathrm{collision}}}} + T_{\mathrm{buffer}}, \tag{S5}$$

where K is the energy-exchange constant and $t_{\mathrm{collision}}$ is the interval of collisions between the clusters and the buffer gas. The interval was obtained as the reciprocal of the Langevin rate constant

$$k_{\mathrm{Langevin}} = \sqrt{\frac{\pi\alpha_{\mathrm{buffer}}e^2}{\varepsilon_0\mu}}\, n_{\mathrm{buffer}}, \tag{S6}$$

where α_{buffer} is the polarizability volume of the buffer gas, e the elementary charge, ε_0 the vacuum permittivity, $\mu = m_{\mathrm{parent}}m_{\mathrm{buffer}} / (m_{\mathrm{parent}} + m_{\mathrm{buffer}})$ the reduced mass, m_{parent} the mass of the parent cluster, m_{buffer} that of the buffer-gas atom and $n_{\mathrm{buffer}} = p_{\mathrm{buffer}} / k_{\mathrm{B}}T_{\mathrm{buffer}}$ the density of the buffer gas. By solving eqns (S2) thru (S6), the density (or population) of the parent cluster is derived as a function of time after laser irradiation. Because it is difficult to solve these equations analytically, eqn (S2) was transformed to the following equation to perform numerical simulation:

$$n_{\text{parent}}(t + \Delta t) - n_{\text{parent}}(t) = -k_{\text{RRK}}(t) n_{\text{parent}}(t) \Delta t, \quad \text{(S7)}$$

where Δt is the time step for the simulation. The temporal change in the population was simulated by solving this equation iteratively until dissociation completes, i.e., all the clusters dissociate or their internal energy becomes lower than the bond-dissociation energy D_0. The values of the parameters used are listed in Table S1.

Table S1 The parameters used in the simulation.

Parameter	Value	Note
ν	4.48×10^{12} Hz	The Debye frequency of bulk silver [a]
D_0	Size-dependent	Bond dissociation energy [b]
$h\nu$	Size-dependent	Absorption maximum
T_{buffer}	300 K	Room temperature
K	4.5 μeV K^{-1}	Value for Pd_{13} [c]
α_{buffer}	$1.38 a_0^3$ *	Value for helium [d]
p_{buffer}	1 Pa	Experimental condition

* a_0 is the Bohr radius. [a] The Debye frequency of bulk silver[10] was adopted for the frequency pre-factor, ν, which is in the same order of the vibrational frequencies of Ag_N^+. [b] Ref. 7. [c] The K value reported for Pd_{13} [9] was employed because that for Ag_N^+ is not available. [d] Ref. 11.

In the following discussion, we compare the decay rate $k_{\text{RRK}}(t)$ (eqn (S3)) with the cooling rate k_{cooling}, which is defined as the reciprocal of the lifetime in eqn (S5):

$$k_{\text{cooling}} = \frac{1}{t_{\text{collision}}} \ln\left(1 - \frac{K}{3Nk_{\text{B}}}\right)^{-1} \quad \text{(S8)}$$

3.2. Results

We first focus on the result of Ag_8^+ (Figure S4). The population of the parent cluster decreased rapidly in an exponential manner: almost all the clusters dissociate within 200 ns. This is because $N = 8$ is sufficiently small to exhibit a dissociation rate of 29 μs^{-1}, which is much higher than the cooling rate of 0.28 ms^{-1}. Therefore, the internal energy and the dissociation rate can be regarded to be constant until dissociation is completed for all the clusters within 200 ns. This result is consistent with the present experiment showing that Ag_8^+ dissociate upon one-photon absorption.

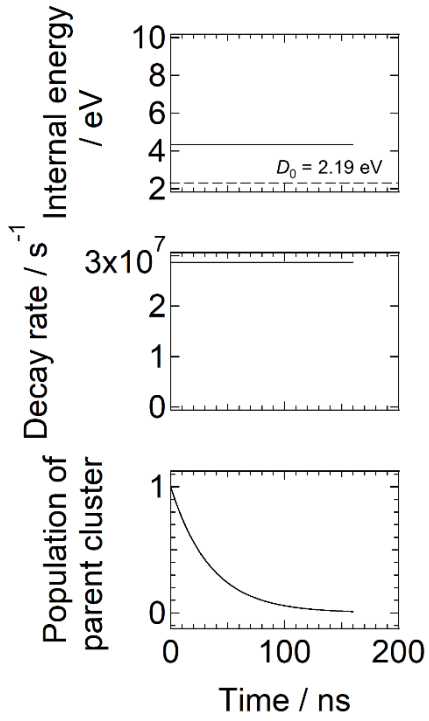

Figure S4. The results of simulation for $N = 8$. The internal energy, decay rate and population of the parent clusters were calculated as a function of time. The dashed line in the top panel indicates the dissociation energy D_0. The photon energy was assumed as 3.87 eV.

On the other hand, Figure S5 shows results of simulation for Ag_{19}^+. Upon one-photon absorption (Figure S5a), the RRK decay rate is much smaller (1.6×10^{-3} s^{-1}) than the cooling rate of 0.12 ms^{-1} at the time origin as shown in the middle panel, which decreases rapidly within 1 ms in accordance with the decrease in the internal energy due to collisional cooling by the buffer gas; the internal energy becomes below the dissociation energy at 10 ms as shown in the top panel. Therefore, dissociation hardly occurs as displayed in the bottom panel. We extended the present simulation to the two-photon process by modeling the internal energy as

$$E_{\mathrm{int}}(t) = \begin{cases} sk_{\mathrm{B}}T_{\mathrm{buffer}} + 2h\nu \equiv sk_{\mathrm{B}}T_{\mathrm{parent}}(0) & (t = 0) \\ sk_{\mathrm{B}}T_{\mathrm{parent}}(t) & (t > 0) \end{cases}. \tag{S9}$$

The result is shown in Figure S5b. It is similar to that of Ag_8^+ in that the population of the parent cluster exhibits an exponential decay, although the time scale of dissociation is longer by about two orders of magnitude. It was thus revealed that two photons are necessary to cause photodissociation for $N = 19$ in an ion trap, which is also consistent with the experiment.

The model can reproduce multi-photon dissociation processes with more than two photons. We simulated dissociation processes of Ag_{41}^+, which dissociated by three-photon absorption in our experiment. The dissociation energy of Ag_{25}^+ in Ref. 7, 2.18 eV, was used in the simulation because there is no data experimentally determined for dissociation energy of Ag_{41}^+. We extended the simulation to the three-photon process in the same manner as the two-photon process:

$$E_{\mathrm{int}}(t) = \begin{cases} sk_{\mathrm{B}}T_{\mathrm{buffer}} + 3h\nu \equiv sk_{\mathrm{B}}T_{\mathrm{parent}}(0) & (t = 0) \\ sk_{\mathrm{B}}T_{\mathrm{parent}}(t) & (t > 0) \end{cases}. \tag{S10}$$

We computed temporal profiles of dissociation yields upon one-, two- and three-photon processes (Figure S6). One- and two-photon processes do not lead to dissociation, while the clusters decay rapidly upon three-photon absorption. Thus, the model presented here

can explain the emergence of multi-photon processes.

The present simulation can also reproduce the dissociation processes of $N = 15$, 17 and 18, which were found to depend on the photon energy. Figure S7 shows the results of the simulation for $N = 18$. The clusters do not dissociate by the low-energy photon at 3.00 eV (Panel a), whereas a part of them dissociate by the high-energy photon at 5.00 eV (Panel b). This photon-energy dependence is consistent with the experimental results. At lower photon energies, the internal energy and the RRK decay rate become lower, which leads to the change in the dissociation process from one-photon to two-photon. At an intermediate photon energy, both one-photon and two-photon processes can occur statistically, which explains the experimental result of Ag_{18}^+ at 4.00 eV shown in Figure S3b.

Note that the results of the present simulation may contain some ambiguity: for example, the energy-exchange constant was employed from Pd_{13}, which was reported in a previous simulation study,[9] because those of Ag_N^+ are not available (see Table S1). Nevertheless, the model proposed here is sufficiently reliable to reproduce the experimental results. The present results of the numerical simulations suggest in turn that the assumption of the frequency pre-factor and the energy-exchange constant are reasonable. The discussion presented here supports the fact that the dissociation takes place statistically, which is manifested also experimentally in the size distribution of fragment ions showing sequential evaporation (see Section 5), while one should note that small clusters may follow non-statistical pathways as reported for Ag_4^+.[12]

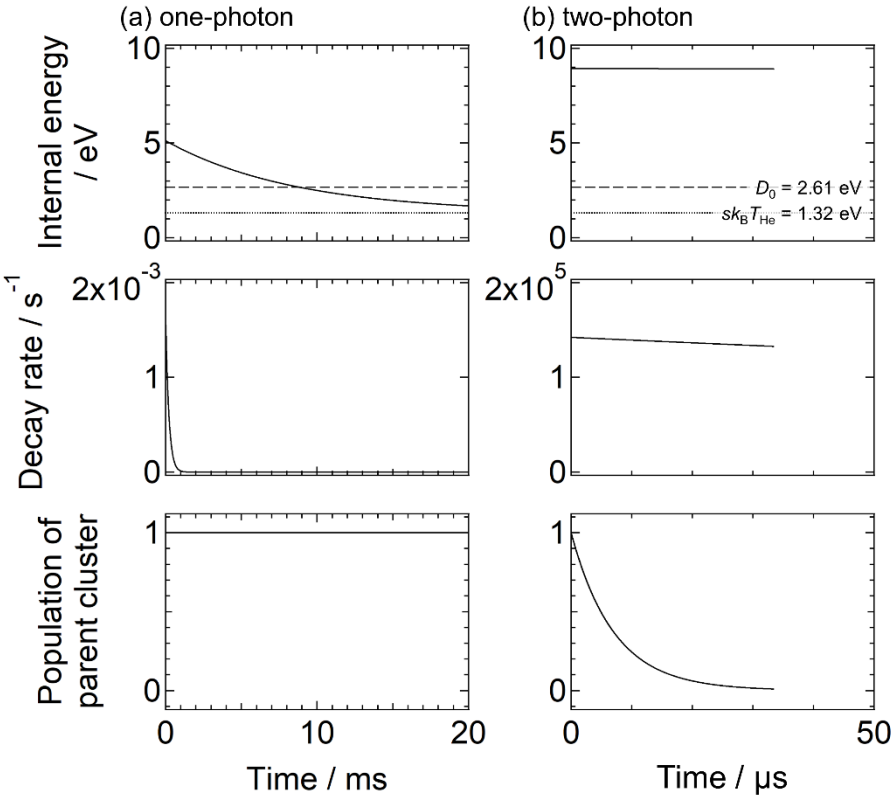

Figure S5. The results of simulation for $N = 19$. Panels (a) and (b) correspond to one- and two-photon processes, respectively. The dashed lines in the top panels indicate the dissociation energy D_0. The dotted lines show the internal energy before irradiation, sk_BT_{He}, i.e., the thermal energy at room temperature. The photon energy was assumed as 3.81 eV.

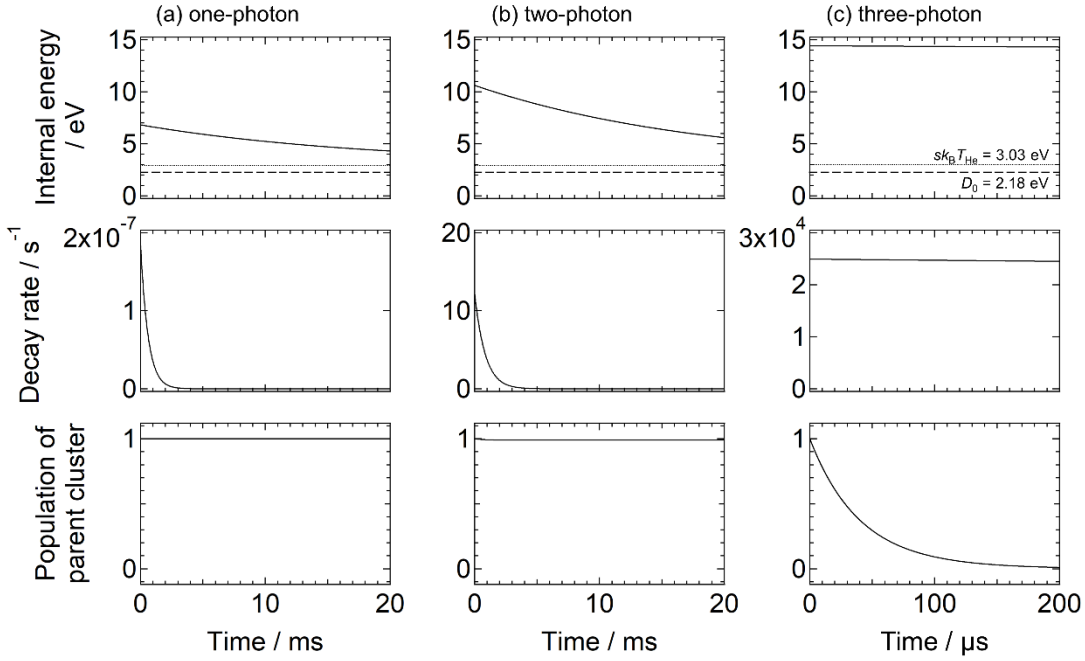

Figure S6. The results of simulation for $N = 41$. Panels (a), (b) and (c) correspond to one-, two- and three-photon processes, respectively. The dashed lines in the top panels indicate the dissociation energy D_0 of Ag_{25}^+, which is the largest size where the dissociation energy is available. The dotted lines show the internal energy before irradiation, sk_BT_{He}, i.e., the thermal energy at room temperature. The photon energy was assumed as 3.80 eV.

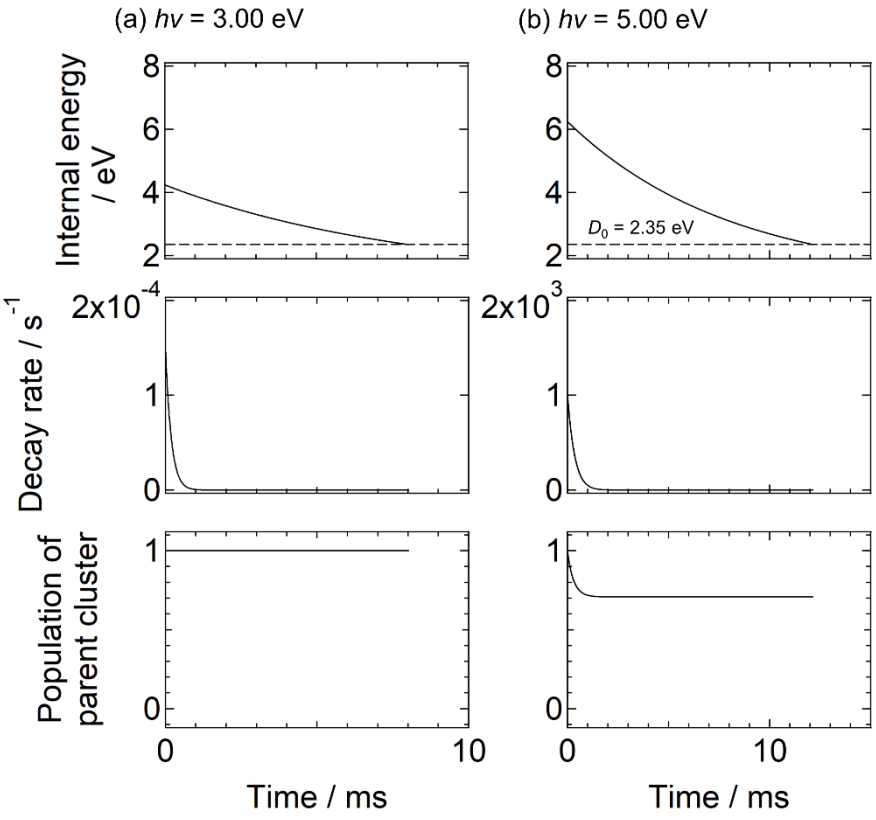

Figure S7. The results of simulation for $N = 18$. One-photon absorption of (a) 3.00 eV and (b) 5.00 eV was assumed by employing eqn (S4).

4. High-sensitivity photoabsorption spectroscopy

4.1. Procedures

Cavity ring-down (CRD) spectroscopy[13] is a powerful technique to measure photoabsorption spectra, detecting extremely weak extinction of light without relying on action spectroscopy that involves destructive processes. The experimental setup and measurement procedures have been described elsewhere.[1,14,15] Briefly, a pair of high-reflectivity mirrors, i.e., an optical cavity, was placed at both ends of the trap as depicted in Figure S8. The reflectivity of the mirrors is typically higher than 99.90% as described in Section 4.2. Laser pulses were introduced into the cavity and thus into the trap after a sufficient amount of cluster ions were loaded. The laser pulses transmitted through the cavity after multiple reflection were detected by a photomultiplier tube, where the temporal profile of the output signal was recorded by an oscilloscope. The signal shows an exponential profile characterized by a decay rate k. Measurement of the decay rate was carried out both with and without ions in the trap, where the difference between the two decay rates, Δk, reflects optical losses due to photoabsorption by the ions. The decay-rate difference, Δk, is related to a photoabsorption cross section, σ_{abs},

$$\sigma_{\mathrm{abs}} = \frac{L_{\mathrm{cavity}}}{cL_{\mathrm{trap}}} \frac{\Delta k}{n_{\mathrm{cluster}}} \tag{S11}$$

where L_{cavity} is the cavity length of 1.6 m, L_{trap} the trap length of 40 cm, c the speed of light and n_{cluster} the density of cluster ions, which was measured in advance as demonstrated in Figure S2. Photoabsorption cross sections were measured as a function of photon energy to obtain a linear photoabsorption spectrum.

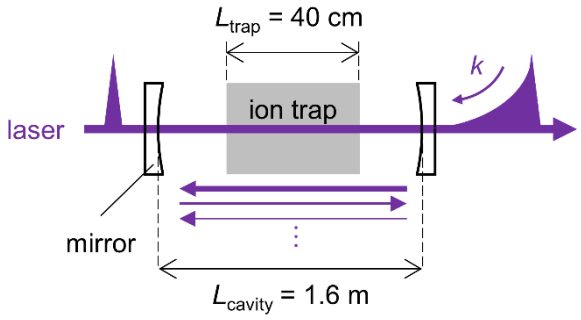

Figure S8. Illustration of cavity ring-down spectroscopy.

4.2. Reflectivity of mirrors

In this technique, reflectivity of the mirrors, R, is the key to high sensitivity; a cavity with a lower loss (a higher finesse) allows higher sensitivity in optical absorption measurement. In our previous studies, we reported that the noise level in absorbance per round-trip of the cavity is as low as 0.1 ppm for R = 99.98%,[1,14,15] which is indeed extremely high sensitivity, whereas it is about 1 ppm for R = 99.90%.[14] Figure S9 shows reflectivity of the present mirrors (LAYERTEC GmbH) as a function of photon energy measured in our experimental setup. We obtained two types of mirrors (mirror A and B) that are tuned at 3.5 and 3.9 eV, respectively. Mirror A shows reflectivity higher than 99.90% in the range between 3.3 and 3.8 eV (375 − 326 nm), while mirror B does between 3.8 and 4.1 eV (326 – 302 nm). The noise level at R = 99.95% was about 0.5 ppm. As the spectrum of Ag_{41}^+, for example, ranges at least from 3.5 to 4.1 eV as shown in Figure 5, the two types of mirrors are really needed to cover the spectral range of interest. It is thus necessary to employ several different types of mirrors to conduct measurement through a broad spectral range.

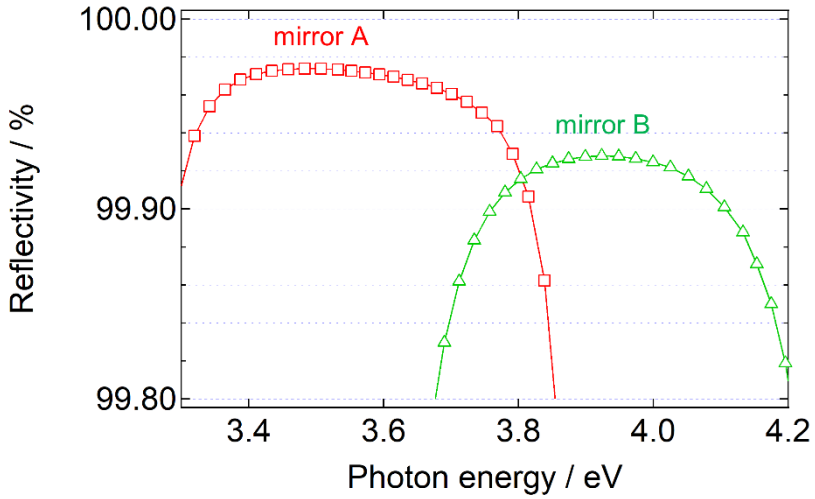

Figure S9. Reflectivity curves of two types of cavity mirrors, A and B, measured in the present experimental setup.

5. Photofragment analysis

Although the measurement of photodissociation yields is sufficient to obtain action spectra, where only parent cluster ions are detected to monitor their depletion upon photoabsorption, analysis of photofragment ions provides us with further information about the photodissociation process. Size distribution of fragment ions was measured by detecting each size one by one by tuning the second quadrupole mass filter.

The results for Ag_N^+ (N = 9, 21 and 50) are shown in Figure S10. From Ag_9^+, which exhibits one-photon dissociation, Ag_8^+ is the major fragment ion produced via one-atom loss from the parent. As for Ag_{21}^+ dissociating with two photons, Ag_{20}^+ and Ag_{19}^+ are the major fragments. Relatively large Ag_{50}^+, dissociating with three photons, produces Ag_{49}^+, Ag_{48}^+, Ag_{47}^+ and further smaller fragment ions with progressively decreasing intensities. The intensities of Ag_{20}^+ and Ag_{48}^+ are weaker than those of neighboring sizes, which is due to odd–even alternation often observed for alkali- and coinage-metal clusters.[16] The overall dissociation processes are thus described by

monomer and dimer evaporation taking place sequentially.[7,17] These evaporation processes are governed by energetics, which rationalizes employing the statistical theory in the present simulation of dissociation processes.[18]

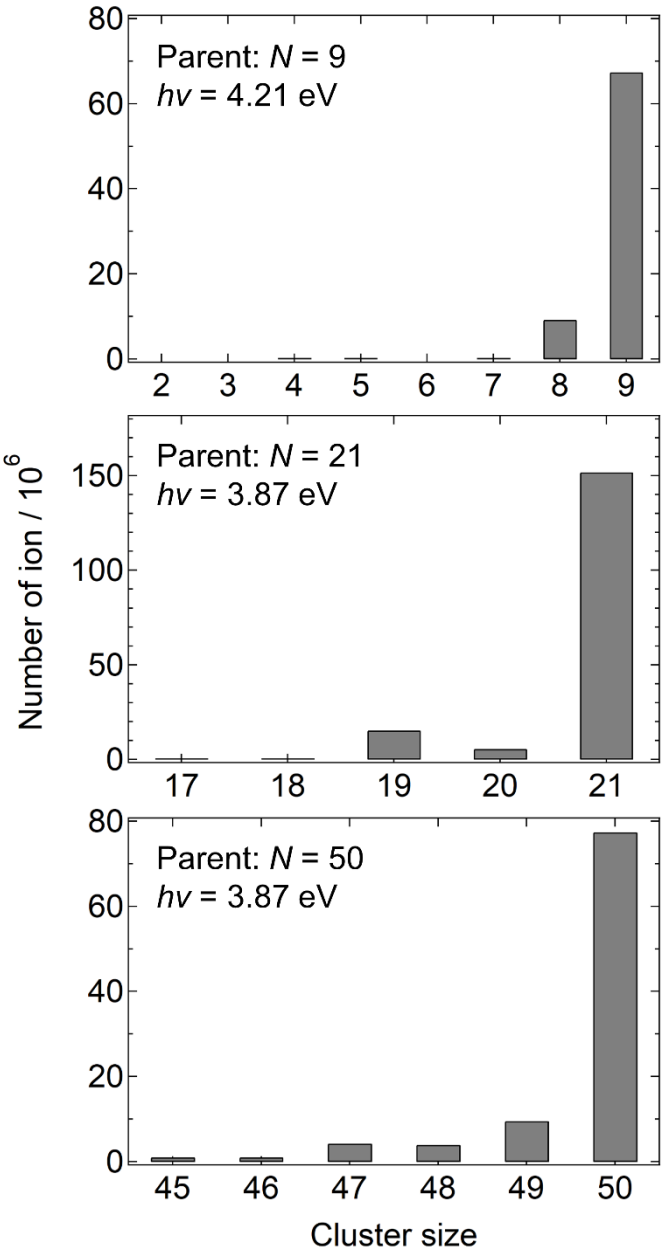

Figure S10. Fragment ions produced upon photodissociation.

References

1 A. Terasaki, T. Majima and T. Kondow, *J. Chem. Phys.*, 2007, **127**, 231101.

2 R. M. Jones and S. L. Anderson, *Rev. Sci. Instrum.*, 2000, **71**, 4335.

3 T. Majima, G. Santambrogio, C. Bartels, A. Terasaki, T. Kondow, J. Meinen and T. Leisner, *Phys. Rev. A*, 2012, **85**, 053414.

4 O. K. Rice and H. C. Ramsperger, *J. Am. Chem. Soc.*, 1927, **49**, 7.

5 L. S. Kassel, *J. Phys. Chem.*, 1928, **32**, 225.

6 J. I. Steinfeld, J. S. Francisco and W. L. Hase, *Chemical Kinetics And Dynamics*, Prentice Hall, Upper Side River, 1989, p. 358.

7 S. Krückeberg, G. Dietrich, K. Lüzenkirchen, L. Schweikhard, C. Walther and J. Ziegler, *J. Chem. Phys.*, 1999, **110**, 7216.

8 U. Hild, G. Dietrich, S. Krückeberg, M. Lindinger, K. Lützenkirchen, L. Schweikhard, C. Walther and J. Ziegler, *Phys. Rev. A*, 1998, **57**, 2786.

9 J. Westergren, H. Grönbeck, S.-G. Kim and D. Tománek, *J. Chem. Phys.*, 1997, **107**, 3071.

10 N. W. Aschcroft and N. D. Mermin, *Solid State Physics*, Saunders College, Philadelphia, 1976, p. 458.

11 M. Masili and A. F. Starace, *Phys. Rev. A*, 2003, **68**, 012508.

12 A. Terasaki, S. Minemoto, M. Iseda and T. Kondow, *Eur. Phys. J. D*, 1999, **9**, 163.

13 A. O'Keefe and D. A. G. Deacon, *Rev. Sci. Instrum.*, 1988, **59**, 2544.

14 A. Terasaki, T. Majima, C. Kasai and T. Kondow, *Eur. Phys. J. D*, 2009, **52**, 43.

15 K. Egashira, C. Bartels, T. Kondow and A. Terasaki, *Eur. Phys. J. D*, 2011, **63**, 183.

16 I. Katakuse, T. Ichihara, Y. Fujita, T. Matsuo, T. Sakurai and H. Matsuda, *Int. J. Mass Spectrom. Ion Processes*, 1985, **67**, 229.

17 U. Hild, G. Dietrich, S. Krückeberg, M. Lindinger, K. Lützenkirchen, L. Schweikhard, C. Walther and J. Ziegler, *Phys. Rev. A*, 1998, **57**, 2786.

18 A. Terasaki, *J. Phys. Chem. A*, 2007, **111**, 7671.